

Supporting Information

Apo ferritin Protein Amyloid Fibrils with Tunable Chirality and Polymorphism

Rocío Jurado¹, Jozef Adamcik², Miguel López-Haro³, Juan Antonio González⁵, Álvaro Ruiz-Arias⁵, Antoni Sánchez-Ferrer², Rafael Cuesta⁴, José M. Domínguez-Vera¹, José J. Calvino³, Angel Orte⁵, Raffaele Mezzenga^{2,6*} and Natividad Gálvez^{1,*}

¹Department of Inorganic Chemistry, Faculty of Sciences, University of Granada, 18071 Granada, Spain

²IFNH, Department of Health Science and Technology, ETH Zürich, 8092 Zürich, Switzerland

³Department of Materials Science and Metallurgical Engineering and Inorganic Chemistry, Universidad de Cádiz, 11510, Cádiz, Spain

⁴Department of Inorganic and Organic Chemistry. E.P.S. Linares, 23700 Linares, Spain

⁵Department of Physical Chemistry, Faculty of Pharmacy, University of Granada, 18071, Granada, Spain

⁶Department of Materials, ETH Zürich, 8093 Zürich, Switzerland

*Correspondence to raffaele.mezzenga@hest.ethz.ch; ngalvez@ugr.es

Table of Contents

Methods	2
Figures:	
S1. TEM images and AFM images of APO fibrils.....	4
S2-3. AFM images and structural characterization of APO fibrils.....	5
S4. CD spectra of APO fibrils.....	6
S5. FTIR spectra of APO fibrils.....	7
S6-9. WAXS scattering profile for APO fibrils.....	8
S10. SDS-PAGE electrophoresis of APO fibrils.....	10
S11-13. MS spectra for APO fibrils.....	11
S14. TEM images of double-stranded horse L-rich APO fibrils.....	14
S15-16. FLIM-PIE imaging of APO aggregates.....	15
S17-18. TEM images, AFM images and SDS-PAGE electrophoresis of functionalized L-rich APO fibrils.....	17
Additional FLIM-PIE results on human L-APO and H-APO aggregates	18
S19-22. FLIM images of human H-APO and L-APO aggregates.....	19

Methods

Samples for Transmission Electronic Microscopy (TEM). All samples (0.1 wt %) were prepared by placing a drop onto a carbon-coated 200 mesh Cu grid. Samples were negatively stained by applying 1 μL of 0.5 % uranyl acetate for 1 min, followed by blotting and drying in air. Electron micrographs were taken with a LIBRA 120 PLUS microscope operating at 120 keV. HR-STEM images were obtained with a FEI TITAN G2 microscope.

Circular Dichroism (CD). All samples (horse L-rich APO fibrils, human L-APO fibrils, and human H-APO fibrils) were previously centrifuged 3 times using Amicon Ultra-4 centrifugal filter devices with a molecular weight cut-off (MWCO) of 50000 Da, and the supernatant was recovered. Another sample was prepared using the native globular horse spleen L-rich APO (0.1 wt % in Milli-Q water). CD spectra of filtered L-rich APO, H-APO and L-APO fibrillar samples and the native globular L-rich APO were recorded using a Jasco J-815 spectropolarimeter equipped with a Peltier-controlled cell holder. Spectra at 20 °C were collected using a precision quartz cell of 2 mm path-length from 190–260 nm with a bandwidth of 1 nm and a scan speed of 50 nm/min. All spectra were recorded by diluting the incubated 0.1 wt % samples 10 times in pH 2 Milli-Q water. Spectra were background subtracted, averaged over 5 scans, and smoothed by OriginPro 8G. The percentages of α -helical and β -sheet contents were determined by writing an algorithm in Excel, using a least-squares adjustment, based on a reference set of more than 150 proteins in the 190–250 nm wavelength range.

Attenuated Total Reflectance Fourier Transform Infrared Spectroscopy (ATR-FTIR). FTIR spectra of all samples were obtained with a Varian 640 FTIR Spectrometer equipped with a Specac Diamond ATR Golden Gate. Sample powders were scanned over the range from 4000 to 400 cm^{-1} with a resolution of 4 cm^{-1} at room temperature and averaged over 64 scans. The percentages of α -helical and β -sheet contents were determined by deconvolution and assignment of the resulting peaks to the corresponding secondary structure.

Wide Angle X-ray Scattering (WAXS). WAXS experiments were performed using a Rigaku MicroMax-002⁺ microfocused beam (4 kW, 45 kV, 0.88 mA) with the $\lambda_{\text{CuK}\alpha} = 0.15418$ nm collimated by three pinhole collimators (0.4, 0.3, and 0.8 mm). The scattered WAXS intensity was collected in transmission mode by a Fujifilm BAS-MS 2025 imaging plate system (15.2 \times 15.2 cm^2 , 50 μm resolution). An effective scattering vector range of 1 $\text{nm}^{-1} < q < 25$ nm^{-1} was obtained, where q is the scattering wave vector defined as $q = 4\pi \sin \theta / \lambda_{\text{CuK}\alpha}$ with a scattering angle of 2 θ .

Preparation of horse spleen L-rich APO fibrils and human L- and H-APO aliquots for gel electrophoresis. Protein solutions (0.1 wt %) were adjusted to the appropriate pH 2 (diluted HCl dissolved in Milli-Q water) before heat treatment (90 °C, glass tubes hermetically sealed). Five aliquots of the samples were collected at times of 30 min, 1 h, 3 h, 9 h and 24 h from the heating onset and quenched immediately in a water–ice bath to arrest at that specific time the conversion of monomers into fibrils. These aliquots were then labeled for the characteristic heating time and stored at 4 °C.

Gel electrophoresis (SDS-PAGE). For each sample, 12 μL of aliquots at 0.1 wt % was mixed with 3 μL of dithiothreitol (DTT) and 15 μL of XT sample buffer 4X (Bio Rad Laboratories). The solutions were then heated 10 min at 90 °C. The 30 μL solutions and the molecular weight (M_w) markers (PageRuler™ Unstained Protein Ladder) were then loaded on 19% stacking gel buffer and separated at 100 V (10 min) and 200 V (40 min). The gel was collected and stained for 30 min in Coomassie blue dye solution (0.1% Coomassie blue R-250, 40% methanol, 10% acetic acid in water) in a closed container

with continuous agitation. This was followed by several destaining steps with a destaining solution (40% methanol, 10% acetic acid) with continuous agitation.

Matrix-Assisted Laser Desorption Ionization Mass Spectrometry (MALDI-MS). Samples (horse L-rich APO fibrils, human L-APO fibrils, and human H-APO fibrils) were previously centrifuged 3 times using Amicon Ultra-4 centrifugal filter devices with a molecular weight cut-off (MWCO) of 50000 Da and the supernatant was recovered. The samples were 5-fold diluted in 1 v/v% TFA and then desalted using a C18 ZipTip (Millipore, MA, U.S.A.), eluted with 2 μ L matrix solution (α -cyano-4-hydroxycinnamic acid (10 mg/mL) dissolved in 50 v/v% acetonitrile/0.5 v/v% TFA), dried, and analyzed by MALDI-MS (MS/MS) in the positive-ion mode. The measurements were performed on the MALDI mass spectrometers Ultraflex II and Autoflex II (both from Bruker, Germany). Based on the masses and the corresponding MS/MS data, the most probable amino acid (AA) sequences and the cleavage sites for some peptides were proposed.

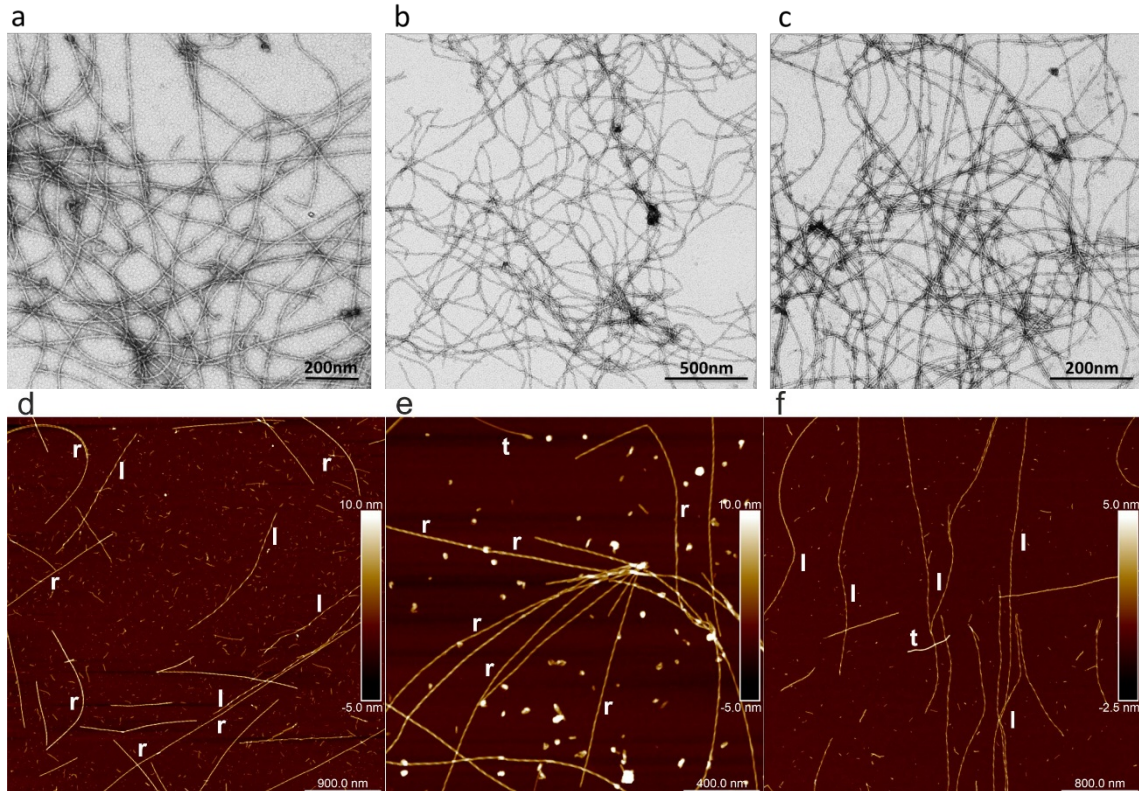


Figure S1. TEM images of (a) horse L-rich APO fibrils, (b) human L-APO fibrils, and (c) human H-APO fibrils. AFM images of (d) horse L-rich APO fibrils, (e) human L-APO fibrils, and (f) human H-APO fibrils. *Note:* r: right-handed fibrils, l: left-handed fibrils, t: tube-like fibrils.

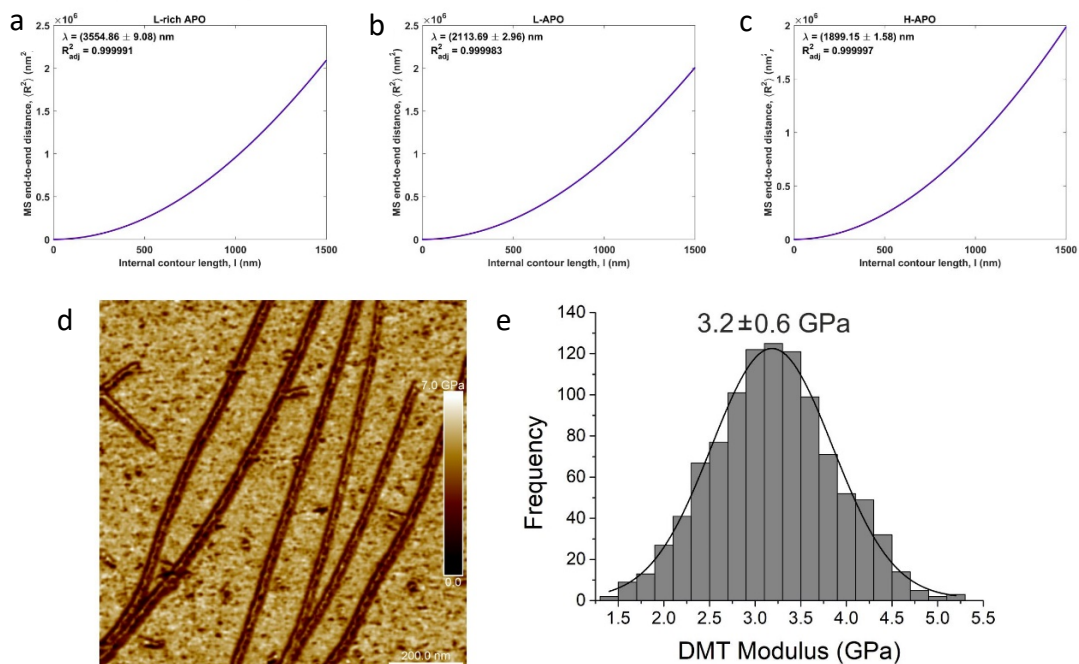


Figure S2. Calculated persistence length for (a) horse L-rich APO fibrils, (b) human L-APO fibrils, and (c) human H-APO fibrils. (d) AFM DMT (Derjaguin, Muller, Toropov) Modulus image with (e) the corresponding distribution of DMT modulus of horse L-rich APO fibrils.

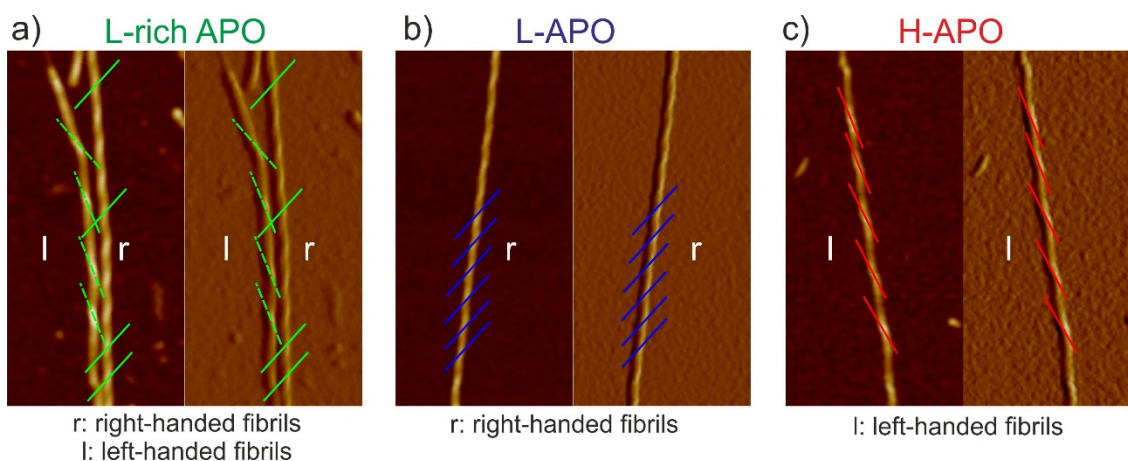


Figure S3. AFM height images (left) with the corresponding AFM amplitude images (right) of (a) horse L-rich APO fibrils, (b) human L-APO fibrils, and (c) human H-APO fibrils showing the chirality of amyloid fibrils. *Note:* r: right-handed fibrils, l: left-handed fibrils.

a)

b)

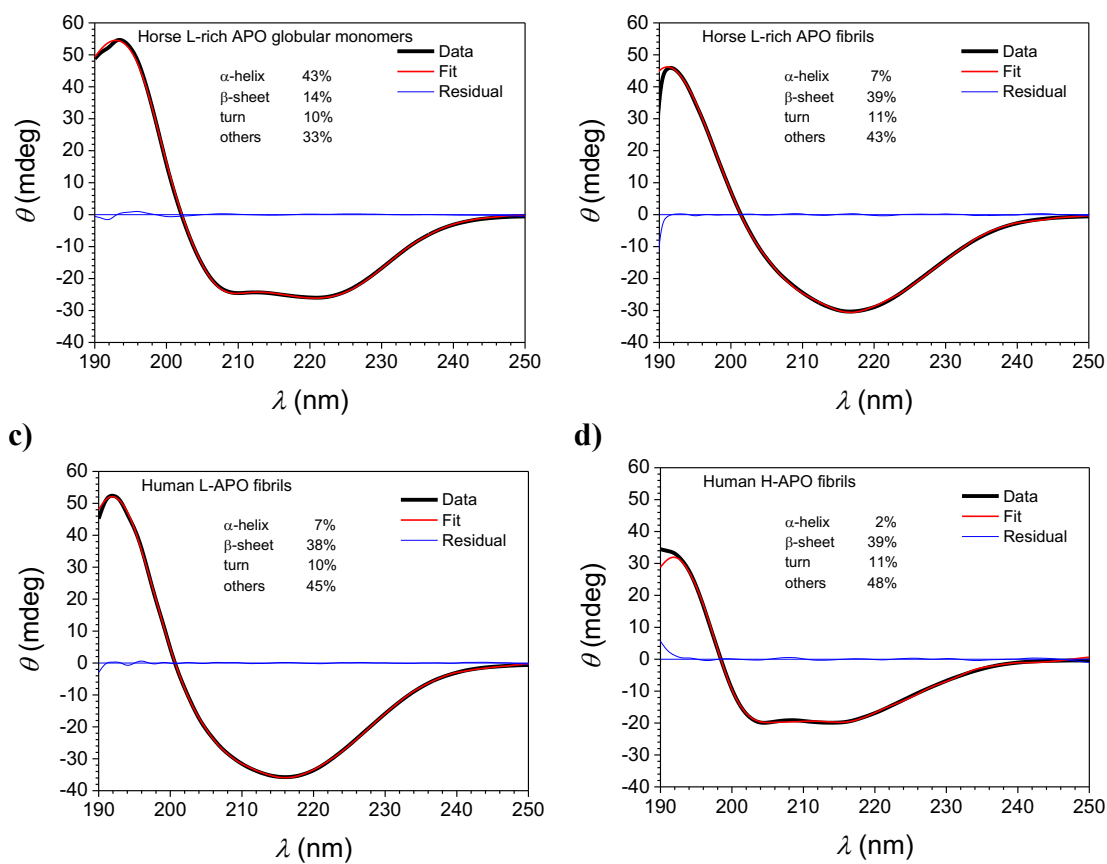


Figure S4. CD spectra with the corresponding fitting analysis of (a) horse L-rich APO globular monomers, (b) horse L-rich APO fibrils, (c) human L-APO fibrils, and (d) human H-APO fibrils.

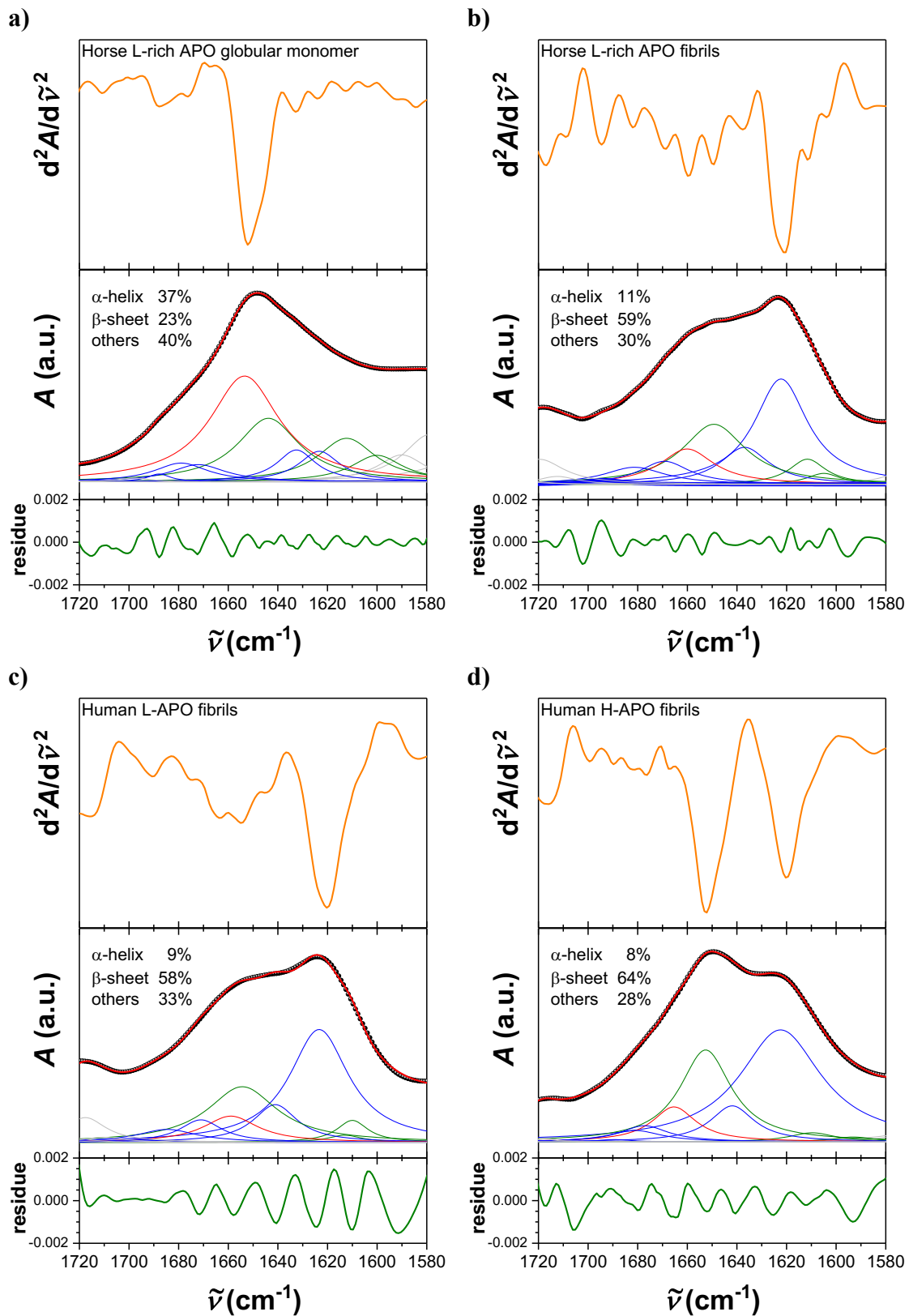


Figure S5. FTIR spectra with the corresponding deconvolution analysis of (a) horse L-rich APO globular monomers, (b) horse L-rich APO fibrils, (c) human L-APO fibrils, and (d) human H-APO fibrils.

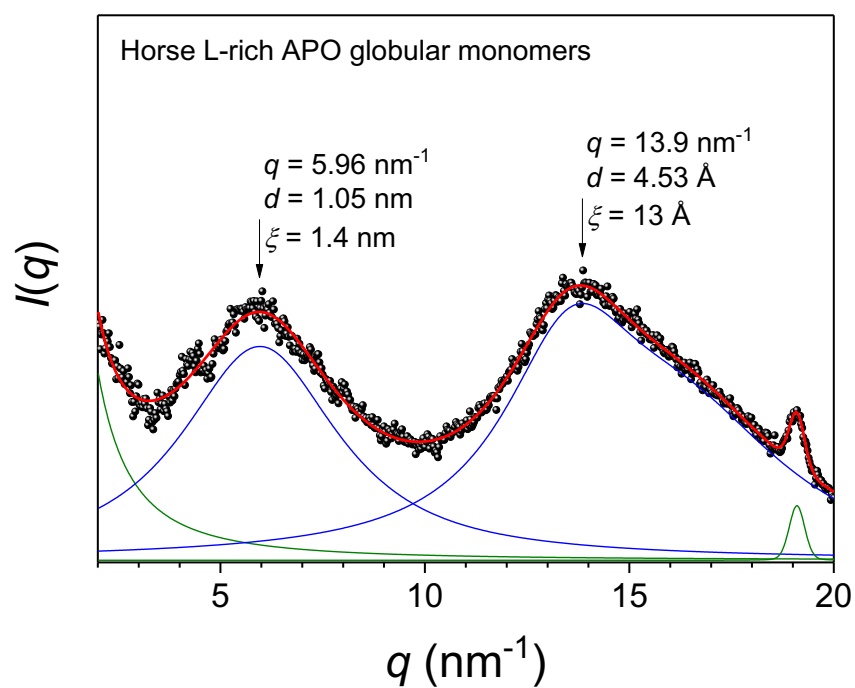


Figure S6. WAXS scattering profile for the horse L-rich APO globular monomers.

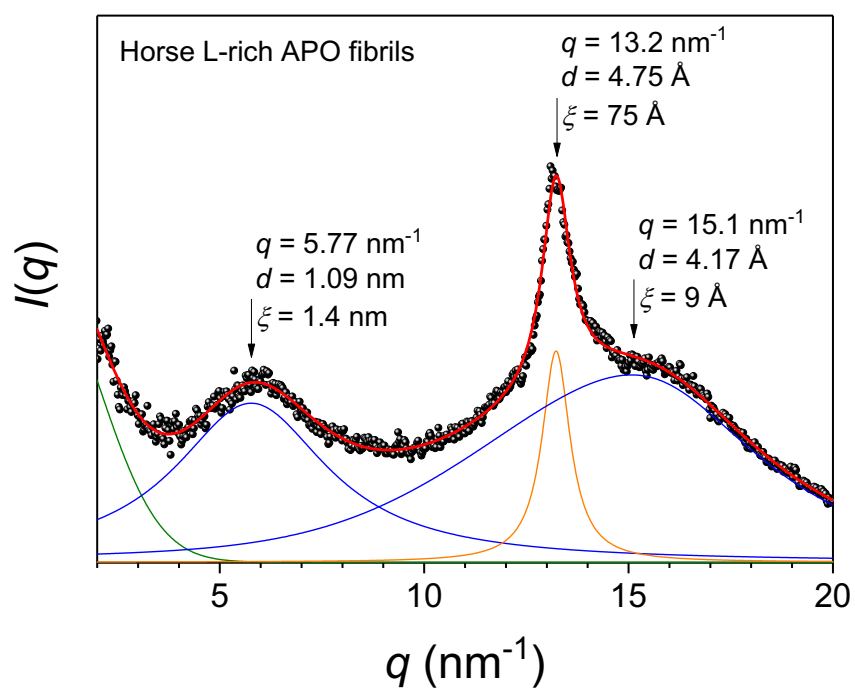


Figure S7. WAXS scattering profile for the horse L-rich APO fibrils.

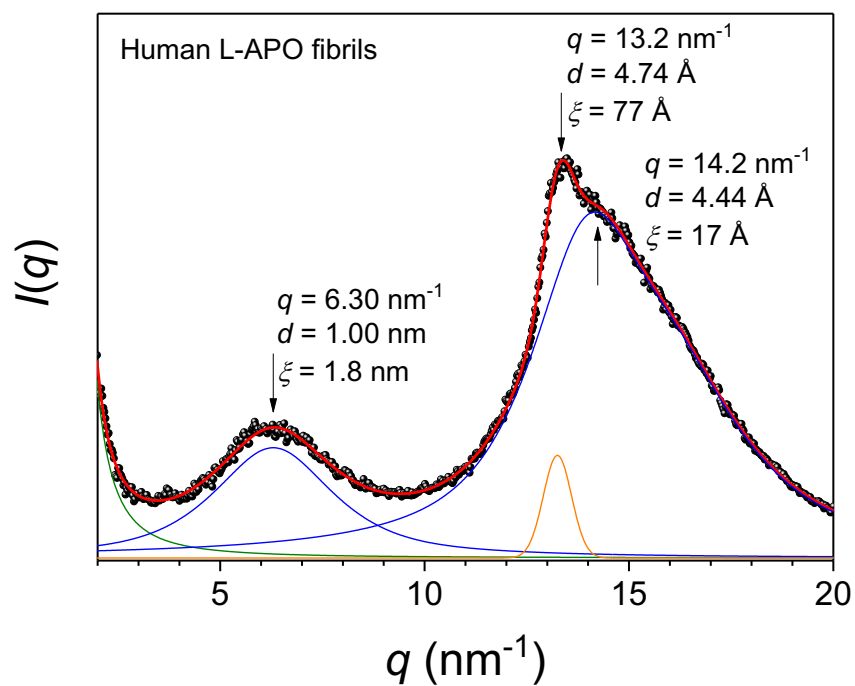


Figure S8. WAXS scattering profile for the human L-APO fibrils.

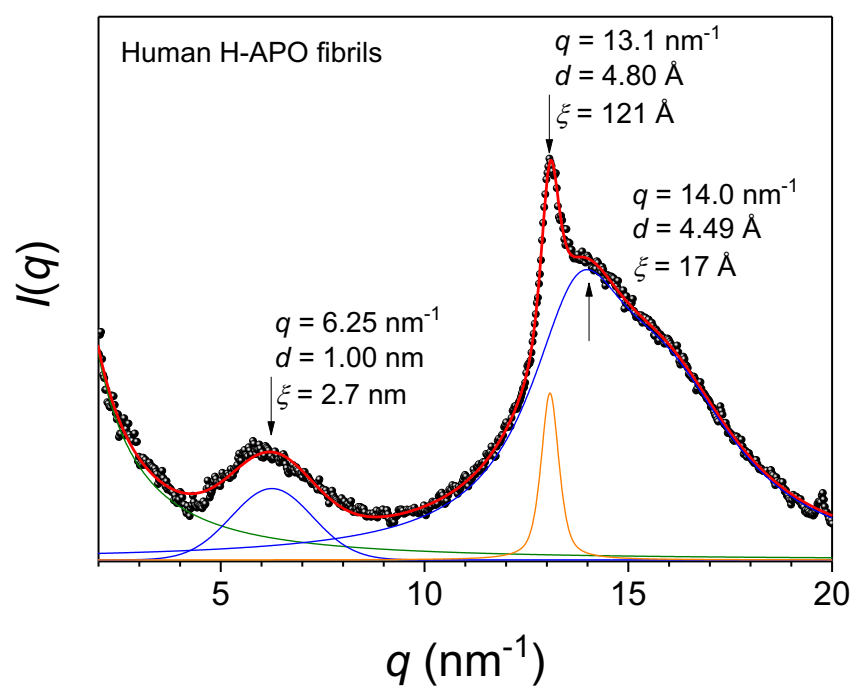


Figure S9. WAXS scattering profile for the human H-APO fibrils.

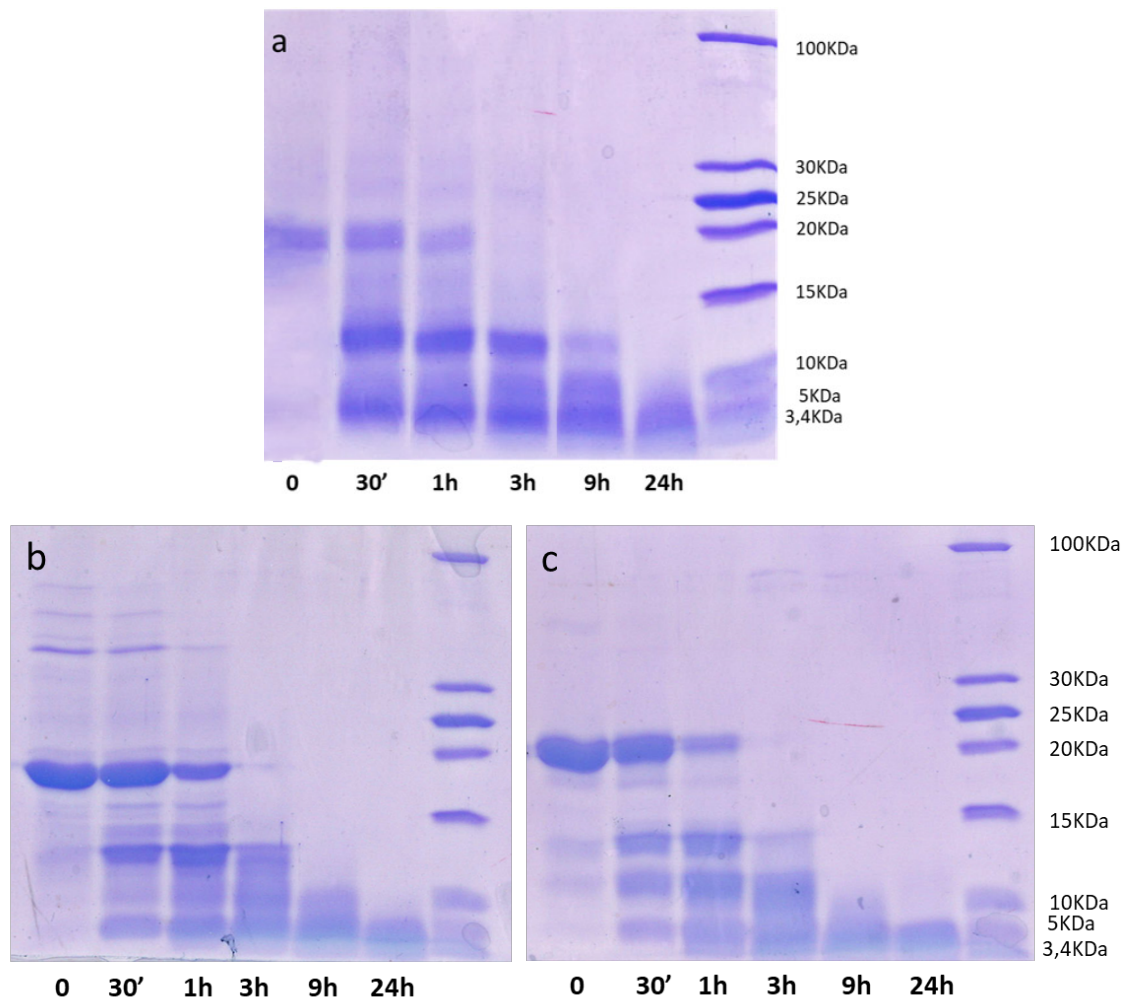


Figure S10. SDS-PAGE electrophoresis of (a) horse L-rich APO fibrils, (b) human L-APO fibrils, and (c) human H-APO fibrils after incubation at different times at pH 2 and 90 °C. The original APO subunit band at 20 kDa disappeared after 3 h, in concordance with the formation of rigid long fibrils. At 24 h of incubation time, the native APO protein is completely hydrolyzed and only low-molecular-weight peptide fragments (<4 kDa) are present in the system.

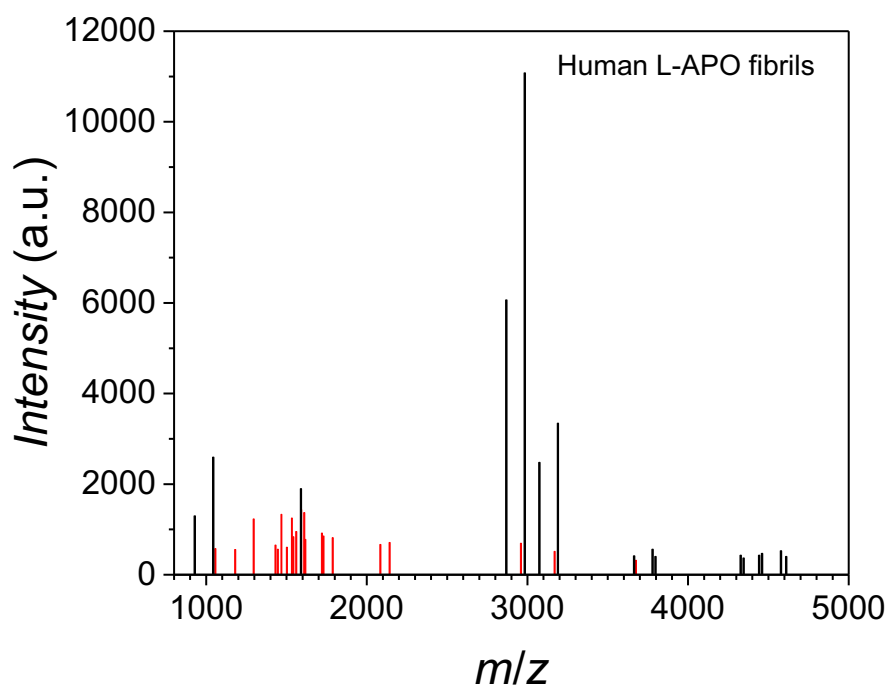


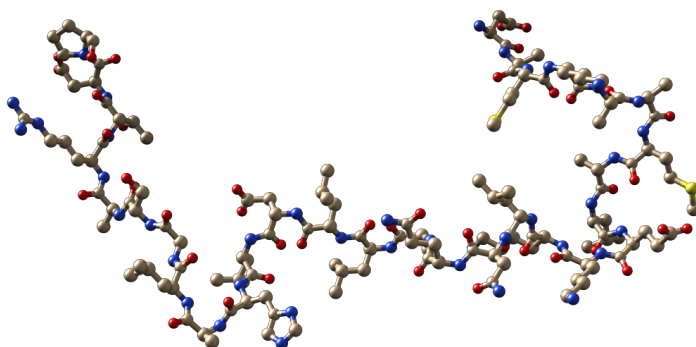
Figure S11. MS spectrum for the human L-APO fibrils showing the identified (black) and not-identified (red) peaks.

Table 2. Identified peaks list compared to L-APO sequence and confirmed by MS/MS.

4%	DLHALGSARTD	9 aa	925 Da	3.2 nm
8%	LDLHALGSARTD	10 aa	1040 Da	3.5 nm
6%	DPHLCDFLETHFLDE	13 aa	1587 Da	4.6 nm
19%	DAMKAAMALEKKNQALLDLHALGSARTD	27 aa	2865 Da	9.5 nm
34%	DAMKAAMALEKKNQALLDLHALGSARTDP	28 aa	2980 Da	9.8 nm
8%	DHLTNLHRLGGPEAGLGEYLFERLTLKHD	27 aa	3071 Da	9.5 nm
10%	DHLTNLHRLGGPEAGLGEYLFERLTLKHD	28 aa	3186 Da	9.8 nm

Chemical structure for **DAMKAAMALEKKNQALLDLHALGSARTDP** 9.8 nm

ASP-ALA-MET-LYS-ALA-ALA-MET-**ALA-LEU-GLU**-LYS-LYS-LEU-ASN-GLN-ALA-LEU-LEU-ASP-LEU-**HIS-ALA-LEU**-GLY-SER-ALA-ARG-THR-ASP-**PRO**



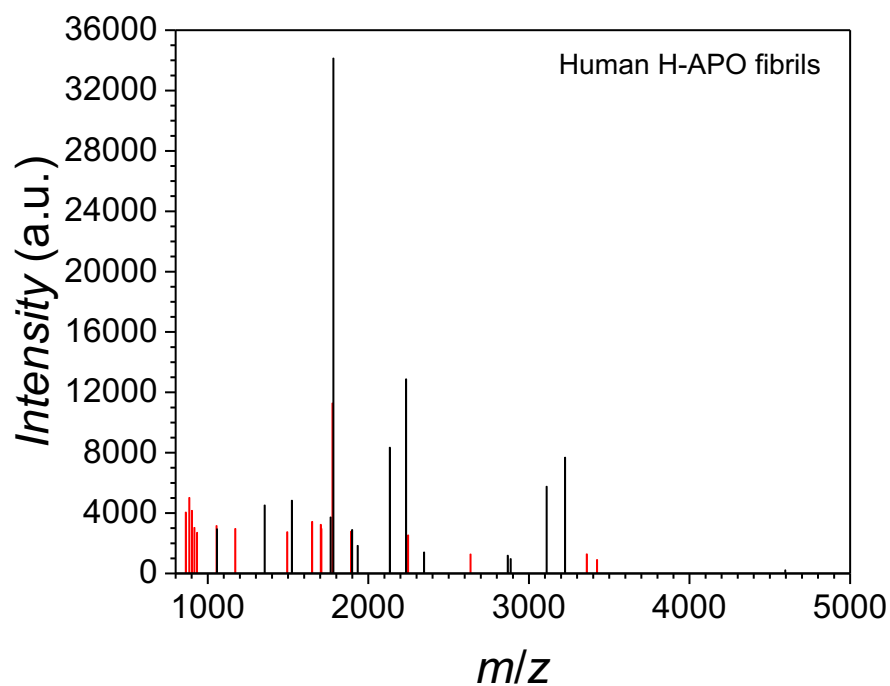


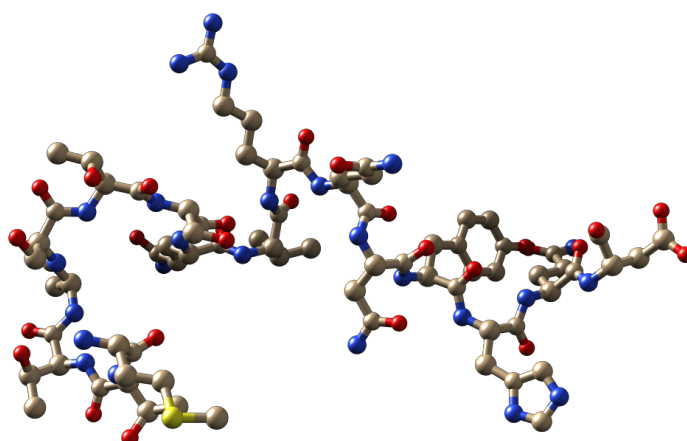
Figure S12. MS spectrum for the human H-APO fibrils showing the identified (black) and not-identified (red) peaks.

Table 3. Identified peaks list compared to H-APO sequence and confirmed by MS/MS.

37%	MTTASTSQVRQNYHQD	15 aa	1781 Da	5.3 nm
9%	DFIETHYLNEQVKAIKELGD	18 aa	2132 Da	6.3 nm
14%	DHVTNLRKMGAPESGLAEYLF	20 aa	2233 Da	7.0 nm
2%	DVALKNFAKYFLHQSHEEREH	19 aa	2345 Da	6.7 nm
6%	DSEAAINRQINLELYASYVYLSMSYF	26 aa	3108 Da	9.1 nm
8%	DSEAAINRQINLELYASYVYLSMSYFDR	27 aa	3224 Da	9.5 nm

Chemical structure for **MTTASTSQVRQNYHQD** 15aa 5.3nm

MET-THR-THR-ALA-SER-THR-SER-GLN-VAL-ARG-GLN-ASN-TYR-HYS-GLN-ASP



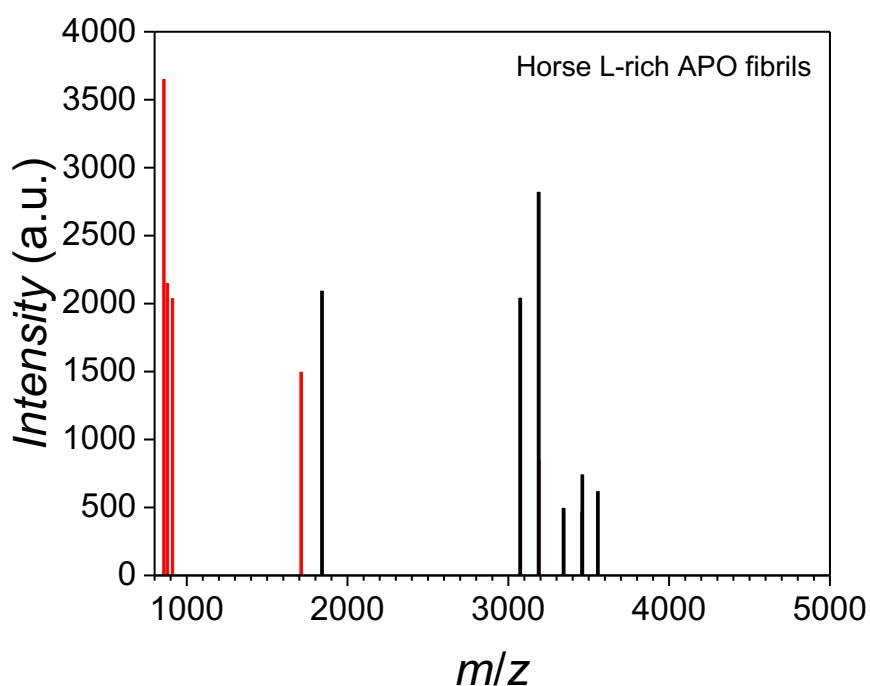


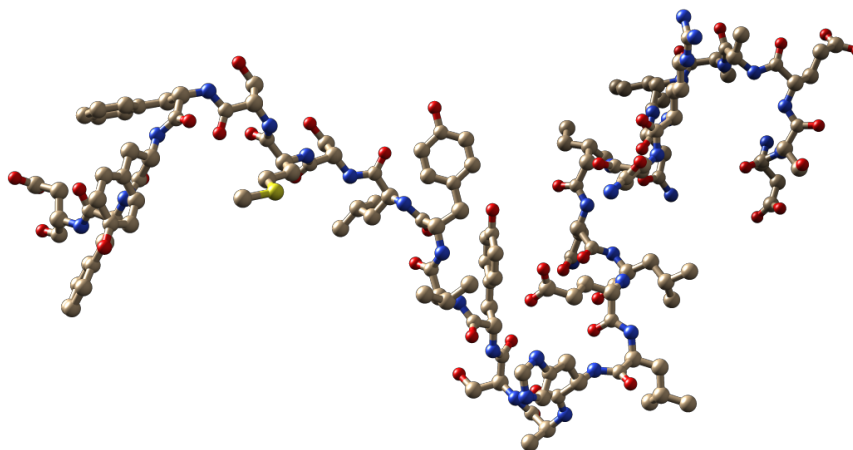
Figure S13. MS spectrum for the horse L-rich APO fibrils showing the identified (black) and not-identified (red) peaks.

Table 1. Identified peaks list compared to L-rich APO sequence and confirmed by MS/MS.

22%	DSEAAINRQINLELHASVYVLSMSFYFD	26 aa	3066 Da	9.1 nm
30%	DSEAAINRQINLELHASVYVLSMSFYFDR	27 aa	3181 Da	9.5 nm

Chemical structure for DSEAAINRQINLELHASVYVLSMSFYFD 26 aa 9.1 nm

ASP-SER-GLU-ALA-ALA-ILE-ASN-ARG-GLN-ILE-ASN-LEU-GLU-LEU-HIS-ALA-SER-TYR-VAL-TYR-LEU-SER-MET-SER-PHE-TYR-PHE-ASP



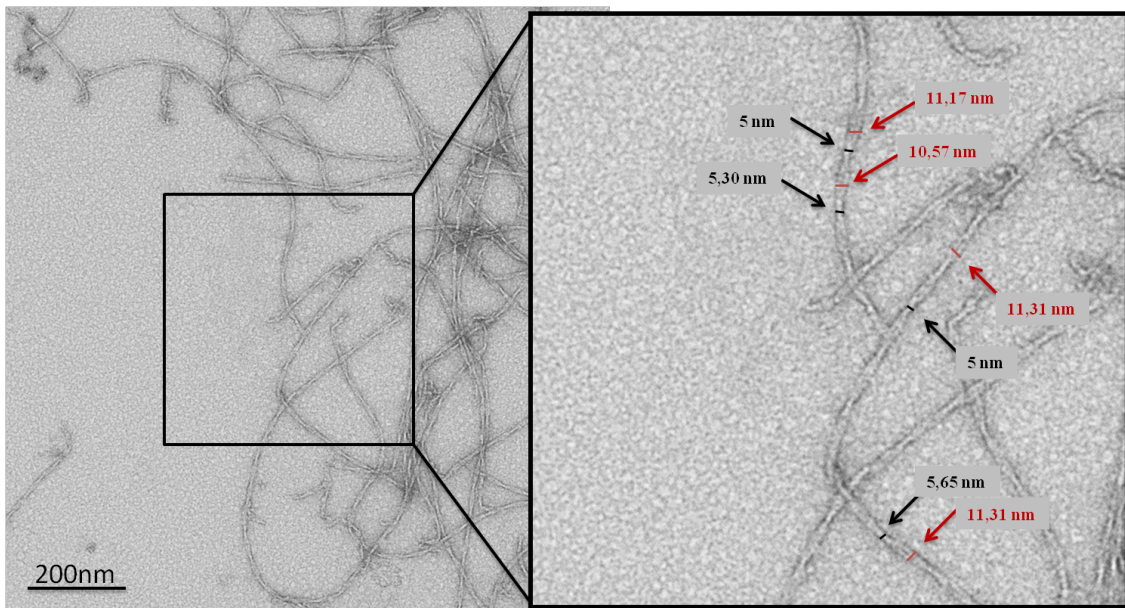


Figure S14. TEM images showing double-stranded horse L-rich APO fibrils. The arrows indicate a width variation with wide zones (red) and thinner zones (black) confirming the presence of two individual protofilaments.

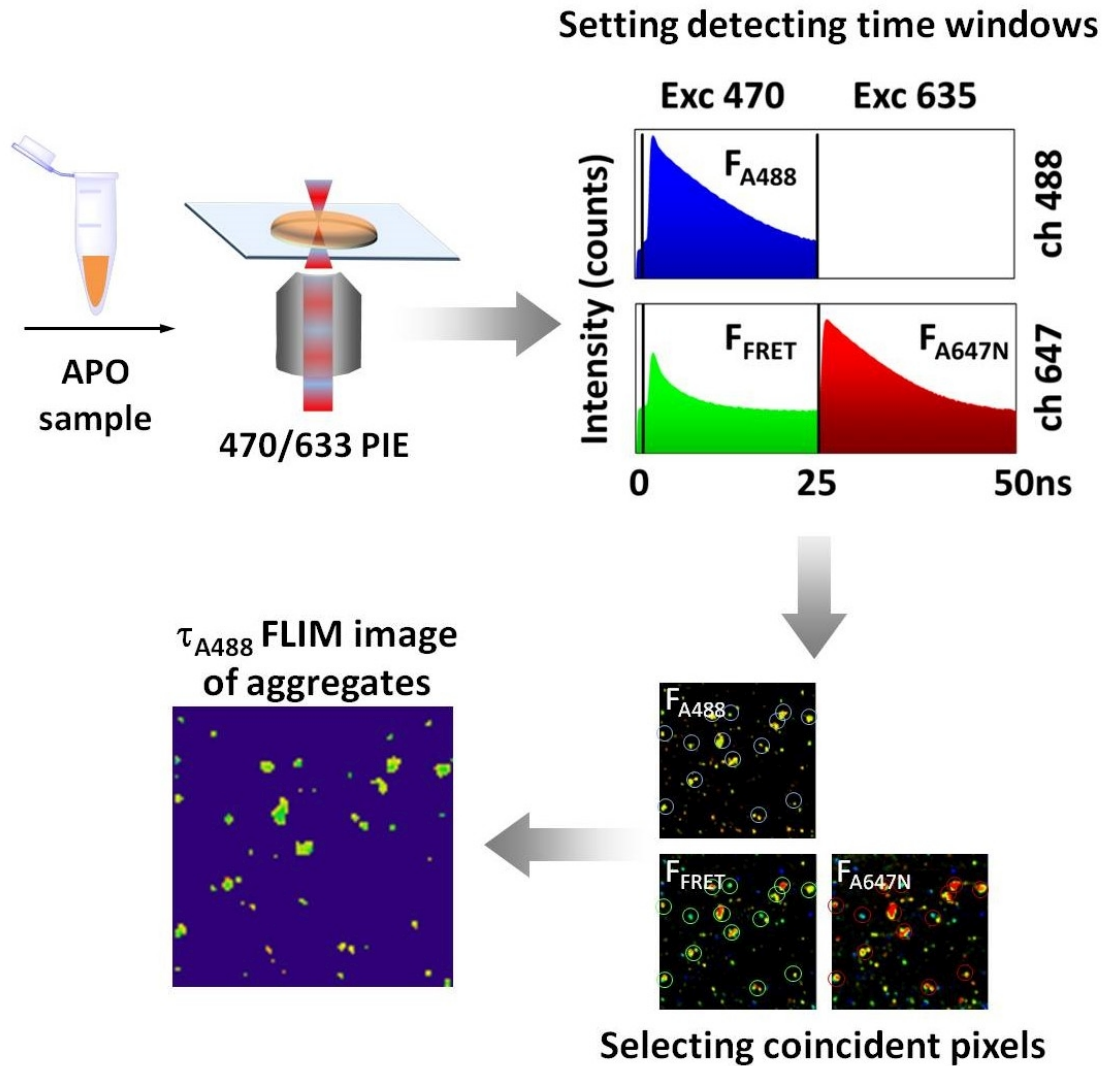


Figure S15. Fluorescence lifetime imaging microscopy with pulsed interleaved excitation (FLIM-PIE) imaging of APO aggregates. Dual-color pulsed interleaved excitation (PIE) was employed to excite both the donor and the acceptor fluorophore in an alternating manner. The fluorescence signal is collected in two different channels (for A488 and A647, respectively). Three different images can be reconstructed by applying adequate time windows: F_{A488} , donor FLIM image; F_{FRET} , FRET image in the acceptor channel when the donor is preferentially excited; and F_{A647N} , directly excited acceptor FLIM image. Aggregates are defined in pixels that exhibit simultaneous intensity in the three channels. Then, a mask is applied in the donor FLIM image for just these pixels, in order to extract the τ_{A488} distributions.

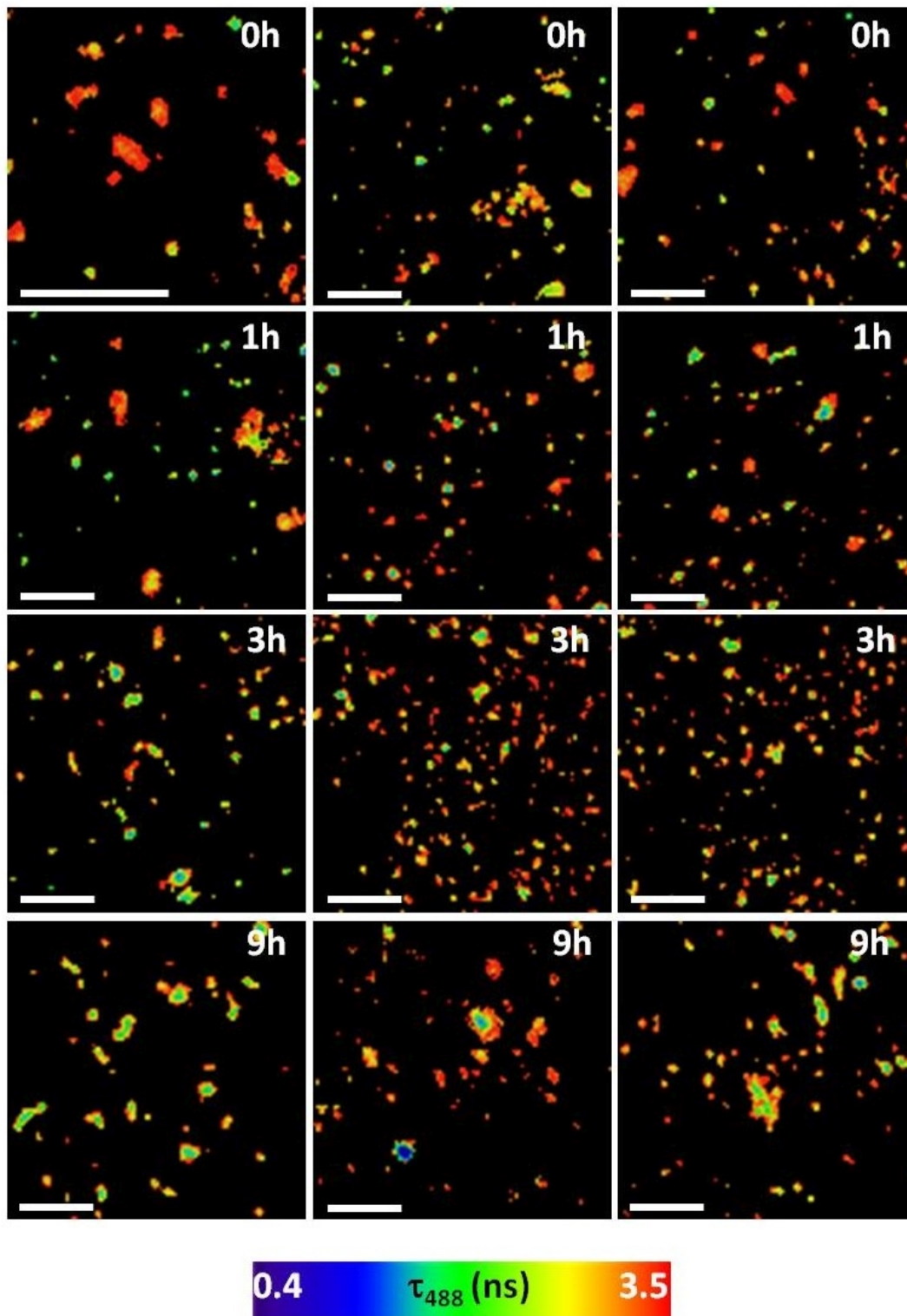


Figure S16. Examples of donor (A488) FLIM images of horse L-rich APO aggregates after different incubation times. Scale bars represent 5 μm .

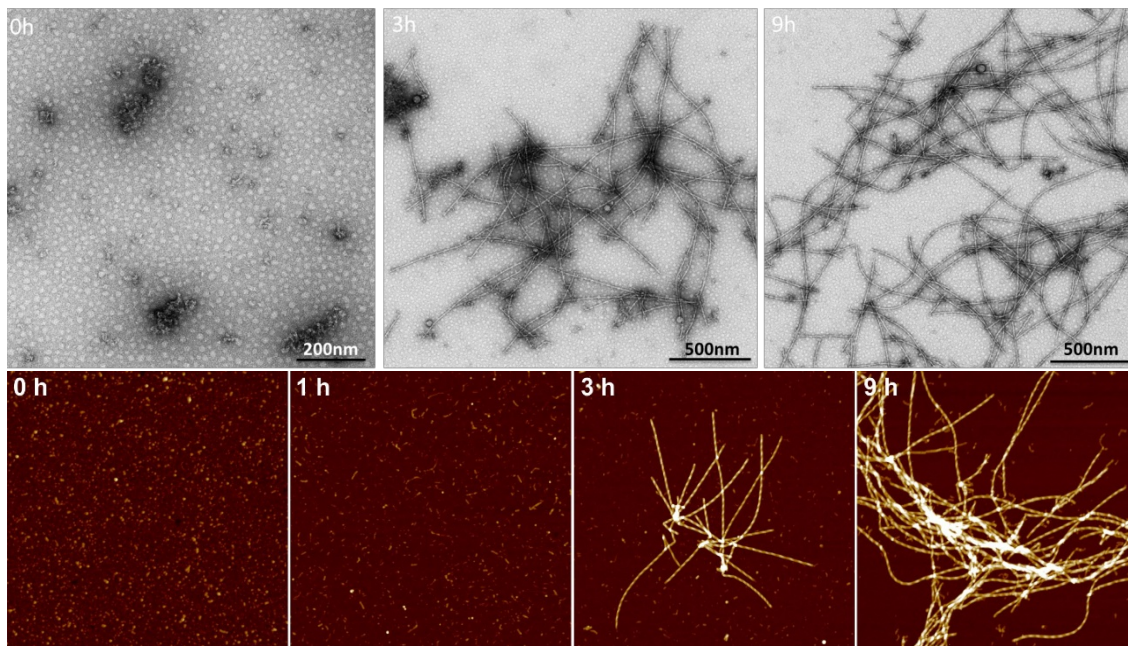


Figure S17. TEM images and AFM height images of A488 and A647-functionalized horse L-rich APO kinetics showing the correct formation of the fibrils. Scale bars in AFM images represent 400 nm.

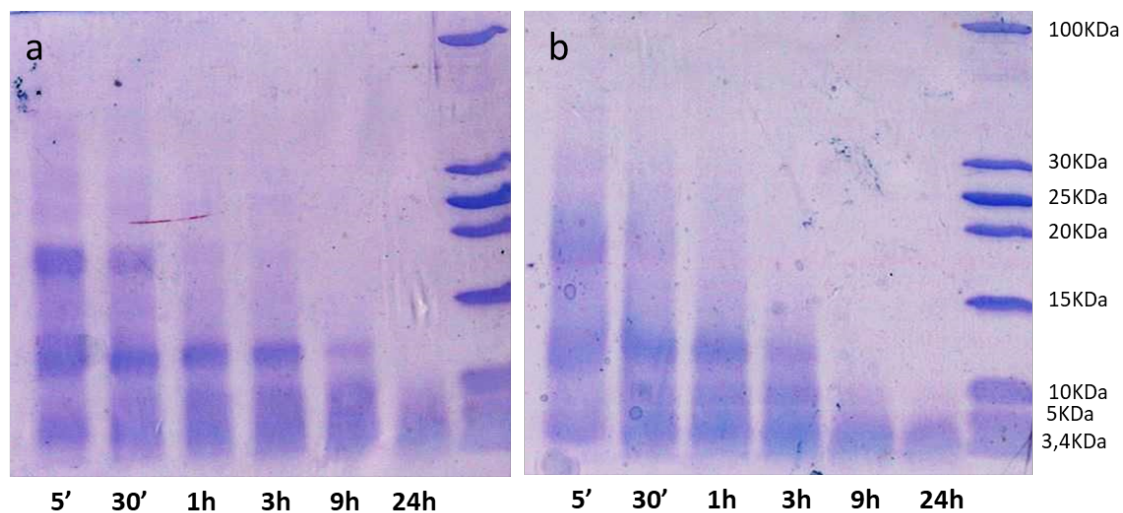


Figure S18. SDS-PAGE electrophoresis of (a) horse L-rich APO fibrils, and (b) A488 and A647-functionalized horse L-rich APO fibrils showing no significance differences.

Additional FLIM-PIE results on human L-APO and H-APO aggregates.

FLIM-PIE is an imaging technique with single-molecule resolution that allows precise identification of different types of oligomers by focusing on the intra-oligomer energy transfer (FRET) from monomers labelled with donor (Atto 488, A488) and acceptor (Atto 647N, A647) fluorophores. The oligomers are unequivocally detected through the simultaneous reconstruction of the donor, FRET, and directly excited acceptor images and the intra-oligomer FRET efficiency, E , is estimated through the donor fluorescence lifetime (τ_{A488}).

The incubation of equimolar mixtures of the donor- and acceptor-labelled human H-APO or human L-APO subunits under fibril formation conditions for several hours resulted in the effective co-aggregation and formation of mature fibrils.

The incubation of human H-APO evidenced different types of aggregates, according to the τ_{A488} values, and thus exhibiting different average FRET efficiencies. The distribution of FRET values appears to vary with the size of the oligomers (Fig. S19a and S20), revealing three dominant populations, a population with $\tau_{A488} > 4$ ns, and hence absence of detectable FRET, probably caused by residual crosstalk; a low-FRET population with $\tau_{A488} = 3.07 \pm 0.09$ ns ($E = 0.23$); and a high-FRET population with $\tau_{A488} = 2.01 \pm 0.09$ ns ($E = 0.50$). The high-FRET population increases its weight as incubation proceeds, whereas the low-FRET population decreases with time (Fig. S19b and S19c).

The behaviour of aggregating human L-APO (Fig. 19d and S21) was similar, but with certain differences to that of human H-APO. The high-FRET population was more abundant in human L-APO, with contributions always larger than 30% (Fig. S19e and S19f). Strikingly, the FRET efficiency of the high-FRET aggregates was around $E = 0.58$, in the first hour of aggregation, but it then decreased to values around $E = 0.43$. This is evidenced by the shift of the population to larger τ_{A488} values with time (Fig. S19e). The low-FRET ($\tau_{A488} = 3.16 \pm 0.16$ ns, $E = 0.21$) and non-FRETting ($\tau_{A488} > 4$ ns) populations showed similar features to that of human H-APO.

To gain more insights into the high-FRET aggregates of human L-APO, the 9 h-incubated solution was filtered, and the remaining insoluble aggregates were imaged. Two populations were mainly found (Fig. S22), exhibiting an average τ_{A488} of 1.74 ns ($E = 0.57$) and 2.57 ns ($E = 0.36$). Therefore, the aggregates that are larger in size, concomitantly exhibit the higher FRET efficiency values.

The presence of aggregates with different compactness, and therefore FRET efficiency, is in line with the heterogeneous nature of the amyloid fibrillization and the formation of fibrils with polymorphism in the final structures. Of particular importance has been the identification of a different aggregation pathway in human L-APO fibrils, which will grow into right-handed fibrils, with respect to left-handed aggregating human H-APO.

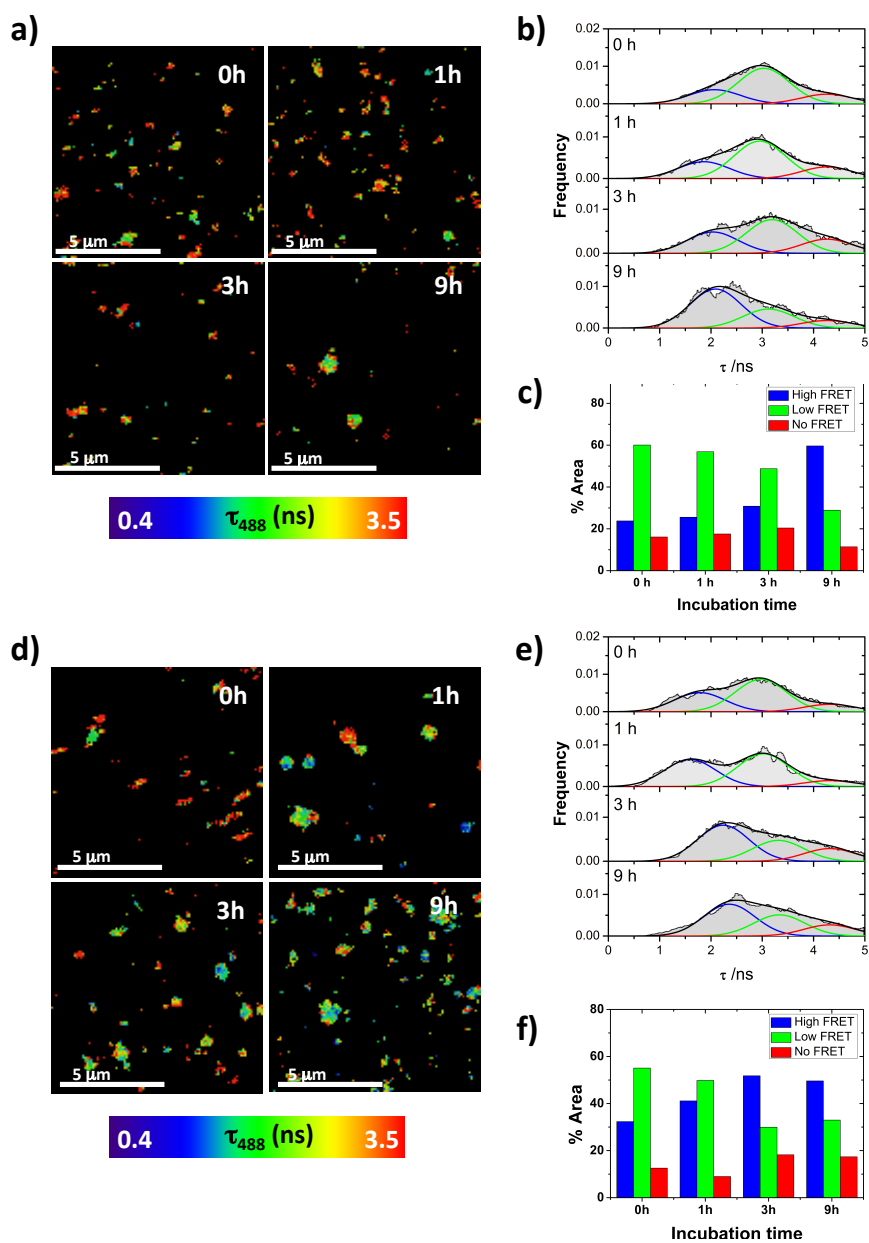


Figure S19. Representative donor (A488) FLIM images of (a) human H-APO aggregates, and (d) human L-APO aggregates after different incubation times. Scale bars represent 5 μm . Frequency histograms of τ_{A488} values in (b) human H-APO aggregates, and (e) human L-APO aggregates, averaged for at least 10 different images. Relative areas of the different peaks obtained in the analysis of the (c) human H-APO and (f) human L-APO histograms.

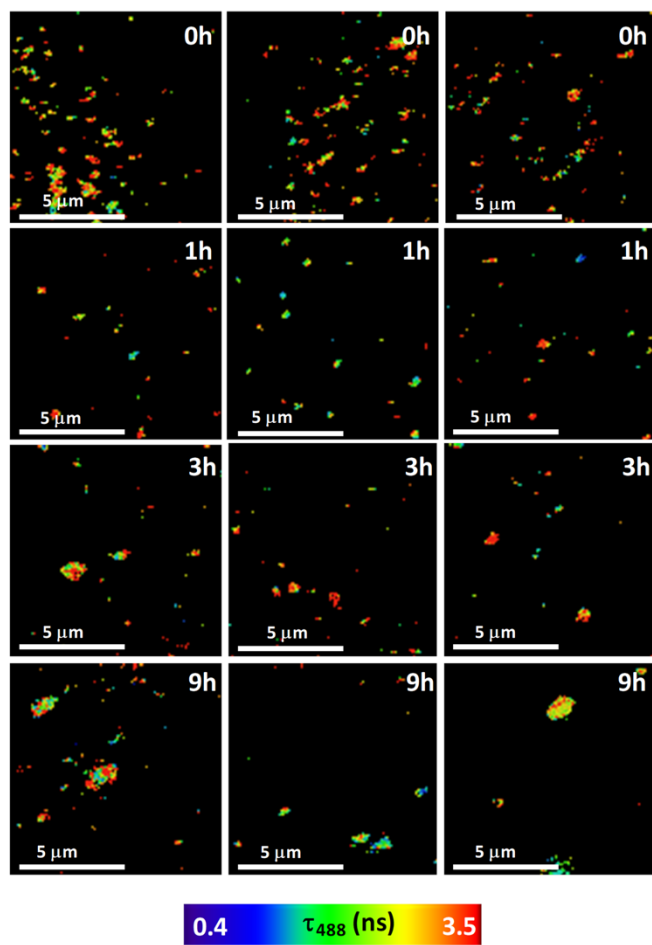


Figure S20. Other representative donor (A488) FLIM images of human H-APO aggregates after different incubation times. Scale bars represent 5 μm .

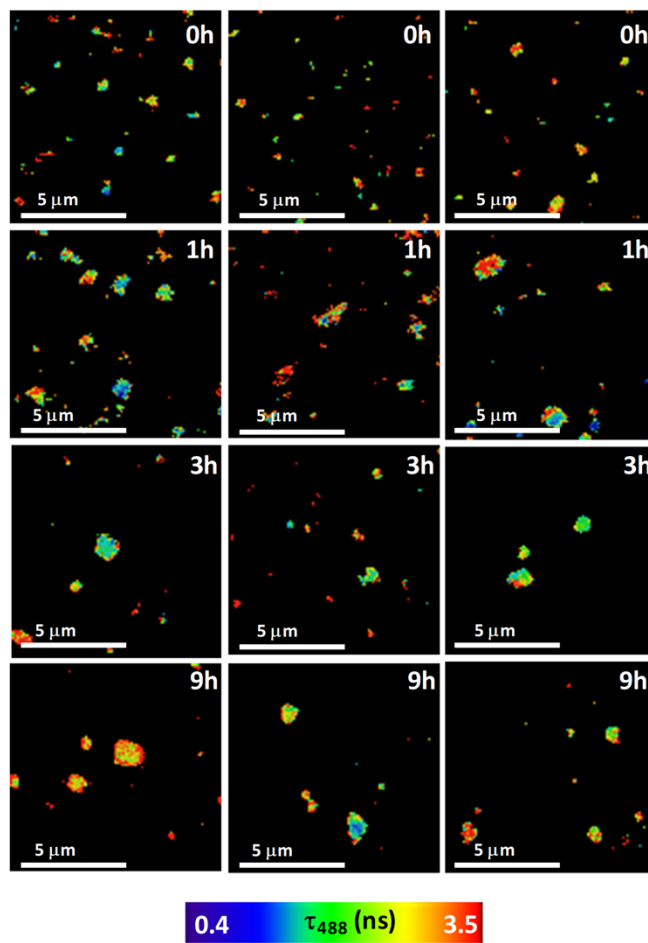


Figure S21. Other representative donor (A488) FLIM images of human L-APO aggregates after different incubation times. Scale bars represent 5 μm.

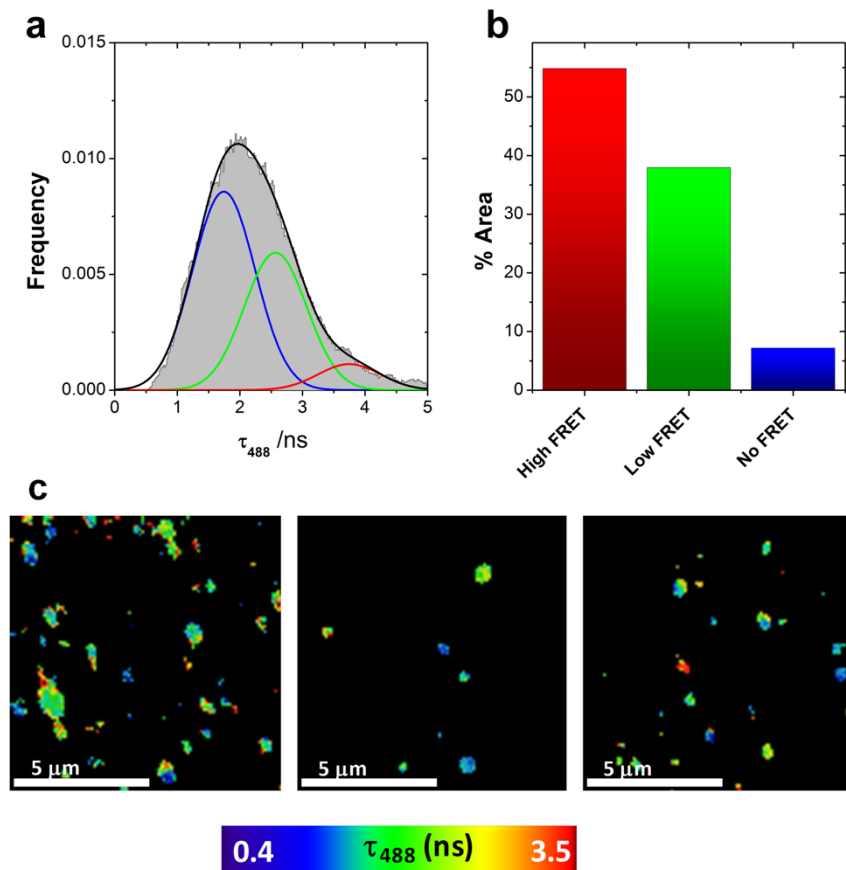


Figure S22. (a) Frequency histograms of τ_{A488} values and (b) the corresponding relative areas of the different peaks obtained in the analysis of the human L-APO insoluble aggregates found in filtered samples, incubated for 9 h. The histogram was averaged for 10 different images. (c) Representative donor FLIM images of insoluble aggregates of human L-APO. Scale bars represent 5 μm .